How to cite: *Angew. Chem. Int. Ed.* **2025**, e202504616
doi.org/10.1002/anie.202504616

Photovoltaic Materials | ***Very Important Paper***

High Performance Electron Acceptors Containing Transition Metals

Zheng Xu[+], Shuhui Ding[+], Wendi Shi, Wenkai Zhao, Xiangjian Cao, Zhaoyang Yao, Yaxiao Guo, Guankui Long, Chenxi Li, Xiangjian Wan, and Yongsheng Chen**

Abstract: A novel molecular platform characteristic of multiple transition metals (CH─Zn, CH─Ni, CH─Pt) on conjugated backbones is first established as high-performance electron acceptors. The CH─Pt-based ternary organic photovoltaics render an excellent power conversion efficiency surpassing 20%, more importantly, the unexplored dependency of central metals on intrinsic physicochemical properties of acceptors, nanoscale morphologies of donor/acceptor blends and final photovoltaic outcomes is fully disclosed. By demonstrating such a rare case of metal-containing acceptor, our work provides insight into whether metal complexes can serve as the building blocks of high-performance acceptors and gives guidance to rational design of metal-containing acceptors.

The power conversion efficiency (PCE) of organic solar cells (OSCs) has transcended 20% thus far,[1–5] largely benefitting from the novel exploration of small molecular acceptors (SMAs).[6–8] However, OSCs are still far behind the first-class silicon/perovskite solar cells,[9–11] especially when comparing their open-circuit voltages (V_{OC}) under the similar bandgaps.[12,13] This is primarily determined by the quite large non-radiative energy loss in OSCs, for example, usually > 0.2 eV for OSCs but only ~0.04 eV for efficient inorganic solar cells.[14,15] Developing SMAs with rigid/planar backbones and constructing their compact/ordered three-dimensional (3D) packing networks have been proven as an effective pathway to suppress non-radiative recombination of excitons or charge transfer (CT) states.[16] Nevertheless, the intrinsically flexible skeleton of organic molecules usually causes the relatively loose and disordered intermolecular packings, which will inevitably expand the density of states, strength the electron coupling between the ground states and excited states (S_1) or CT states, and ultimately make the reduction of energy losses in OSCs quite challengeable.[17,18]

Limited by the above nature of organic materials, the pioneered exportation of SMAs is encountering an insurmountable bottleneck.[19–22] How to introduce innovative photoelectric mechanisms while maintaining the favorable 3D stacking network of molecules[23,24] is particularly important. The organic metal complexes have some unique advantages[25,26] of 1) the d orbitals of transition metal atoms could usually effectively re-align with the π orbitals of aromatic groups, which is beneficial for electron delocalization; 2) the spin–orbit coupling of heavy metal atoms easily forms triplet excitons, which significantly increases the lifetime of molecular excited states and the diffusion length of excitons; 3) metal–metal interactions may enhance intermolecular stacking, promote the intermolecular dynamic relaxation delocalization of photogenerated excitons. Despite these significant advantages, very rare high-performance SMAs containing transition metals have been constructed thus far,[27,28] which is largely determined by the great difficulties in molecular synthesis, more importantly, the reservation of desirable 3D intermolecular packing networks after introducing metal complexes.

Herein, a novel SMA platform characteristic of multiple transition metals (CH─Zn, CH─Ni, CH─Pt) on conjugated backbones, is first established by employing porphyrin–metal complexes as central units (Figure 1a). A systematic investigation including density functional theory (DFT) calculation, single crystal cultivation, nanoscale morphology analysis, etc. has been carried out to disclose the unexplored dependency of central metals on intrinsic photoelectronic properties of SMAs. Finally, CH─Pt-based ternary OSCs render an excellent PCE surpassing 20%, much better than other metal-containing or metal-free SMA counterparts. Our work displayed a rare case of metal-containing SMAs and explored in depth whether metal complexes are promising candidates for building high-performance SMAs.

In order to incorporate organic metal complexes into the molecular skeleton, the electron-rich and planar porphyrin was fused with the widely used S,N-heteroacene of Y-series SMAs,[29–31] rendering a model SMA platform of CH─H (Figure 1a). By coordinating with different open or closed shell metals of Zn, Ni, and Pt, a rare series of SMAs containing

[*] Z. Xu[+], S. Ding[+], W. Shi, X. Cao, Z. Yao, C. Li, X. Wan, Y. Chen
State Key Laboratory and Institute of Elemento-Organic Chemistry, The Centre of Nanoscale Science and Technology and Key Laboratory of Functional Polymer Materials, Renewable Energy Conversion and Storage Center (RECAST), College of Chemistry, Nankai University, Tianjin 300071, China
E-mail: zyao@nankai.edu.cn
yschen99@nankai.edu.cn

Y. Guo
State Key Laboratory of Separation Membranes and Membrane Processes, School of Chemistry, Tiangong University, Tianjin 300387, China

W. Zhao, G. Long
School of Materials Science and Engineering, Nankai University, Tianjin 300350, China

[+] Both authors contributed equally to this work.

Additional supporting information can be found online in the Supporting Information section

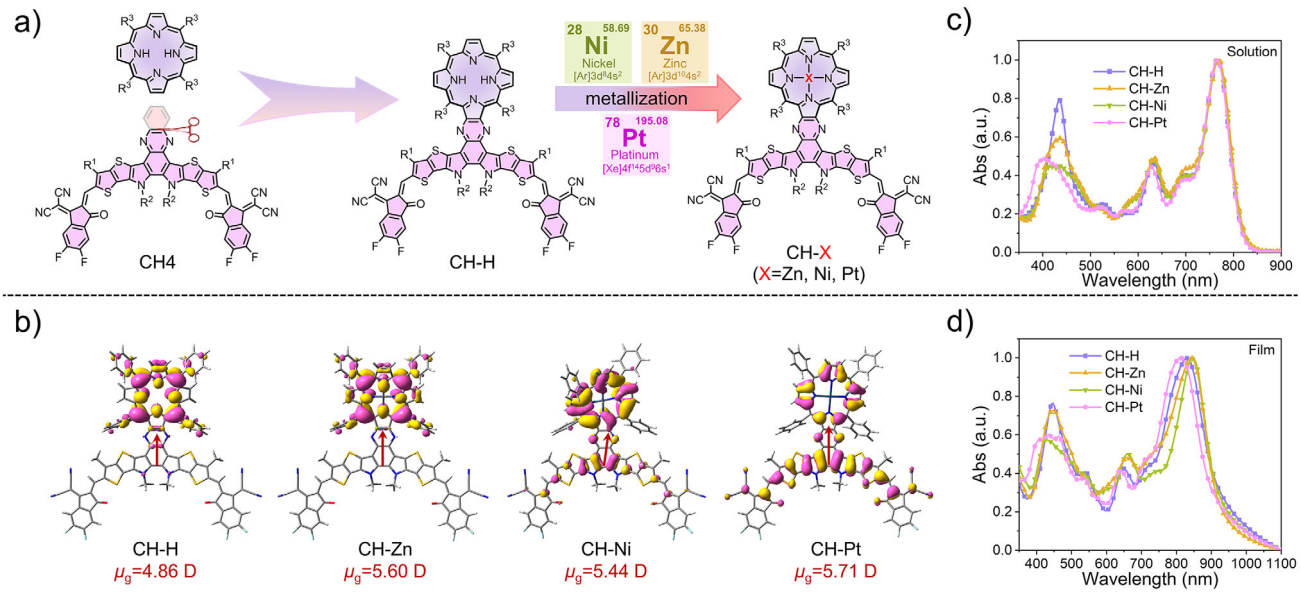

Figure 1. a) Chemical structures of CH—H, CH—Zn, CH—Ni and CH—Pt. b) Calculated HOMOs distribution and dipole moments. c,d) Electronic absorption of SMAs in chloroform solutions and solid films, respectively.

organic metal complex were established delicately. DTF calculations reveal the relatively planar molecular geometries of SMAs except that of CH—Ni (Figure S1).[32] The lowest unoccupied molecular orbitals (LUMOs) of SMAs show the similar locations on whole molecular backbones and reach the maximum probability on cyano groups, which is exactly the same as the conventional SMAs, like Y6 and CH4 (Figure S2).[8,33] However, it is interesting that the highest occupied molecular orbitals (HOMOs) mainly localize on the porphyrin rings for CH—H and CH—Zn, but expand to the S,N-heteroacene for CH—Ni and CH—Pt, especially for CH—Pt that distributing on the whole porphyrin and S,N-heteroacene skeletons (Figure 1b). Note that the spatial separation of HOMOs and LUMOs may result in a significantly reduced energy offset (ΔE_{ST}) between singlet and triplet states (Table S1), providing a potential energy loss saving pathway similar to thermally activated delayed fluorescence (TADF) mechanism.[34] Actually, we think TADF phenomenon may be very difficult to be observed/confirmed directly in such a complicated organic photovoltaic device, especially for the near-infrared systems. However, the planar molecular backbone and sufficient overlap of frontier molecular orbitals for CH—Pt will undoubtedly contribute to the enlarged molar extinction coefficients of 2.07×10^5 M^{-1} cm^{-1} in solutions and 1.71×10^5 cm^{-1} in films, comparing to 1.94–2.04×10^5 M^{-1} cm^{-1} and 1.50–1.64×10^5 cm^{-1}, respectively, for its counterparts (Figure S3). CH—Pt also demonstrate the largest relative dielectric constant and smallest exciton binding energy, moreover, the smallest reorganization energy and largest electron mobility (μ_e) among these SMAs, which is helpful for more efficient charge generation/transport (Figures S4–S6 and Table S2).

The metal coordination downshifts the HOMOs of SMAs gradually through a different degree of ligand–metal charge transfer (LMCT) effects,[35,36] which makes SMAs match the high-performance polymeric donors better at least from the perspective of energy levels (Figure S7). In addition, the dipole moment increases greatly after introducing porphyrin ring (4.86 D for CH—H and only 1.63 D for CH4, Figures 1b and S8), and further increases to 5.3–5.7 D by coordinating central metals. The larger dipole moment is conducive to forming desirable molecular packings and yielding facilitated photodynamic processes in some cases.[37,38] Figure 1c displayed the very similar maximum absorption peaks of SMAs around 768 nm in solutions, which should originate from the strong intramolecular charge transfer (ICT) between S,N-heteroacene central donor and indandione-based terminals. The sharp peak around 437 nm of CH—H is the distinctive absorption of porphyrin, whereas the broader peaks around 420 nm for metal-containing SMAs are also caused by the LMCT effect.[39,40] The shape of absorption spectra changes a lot from solutions to films (Figure 1d), suggesting the quite different molecular packings caused by the variation of central metals.[41,42] This also agrees with the different energy level alignment derived from cyclic voltammetry measurements of SMA films (Figures S9 and S10).

Scheme 1 shows the synthesized routes to SMAs. Note that all SMAs could be afforded with moderate and even good yields, meanwhile, exhibit an excellent thermal stability (Figure S11). Several trials of single crystal cultivation successfully provided two crystals of metal-free CH—H and Zn-containing CH—Zn (Table S3, CCDC number: 2422130 for CH—H and 2422137 for CH—Zn). As expected, both CH—H and CH—Zn possess a relatively planar molecular geometry as shown in Figure S12. Excitingly, the featured 3D intermolecular packing network similar to the state-of-the-art Y-series acceptors, which is regarded as a key factor of the improved photodynamic processes,[43,44] could be still achieved despite the great structural changes of central units (Figure 2a,b). Although the four phenyl groups grafted on

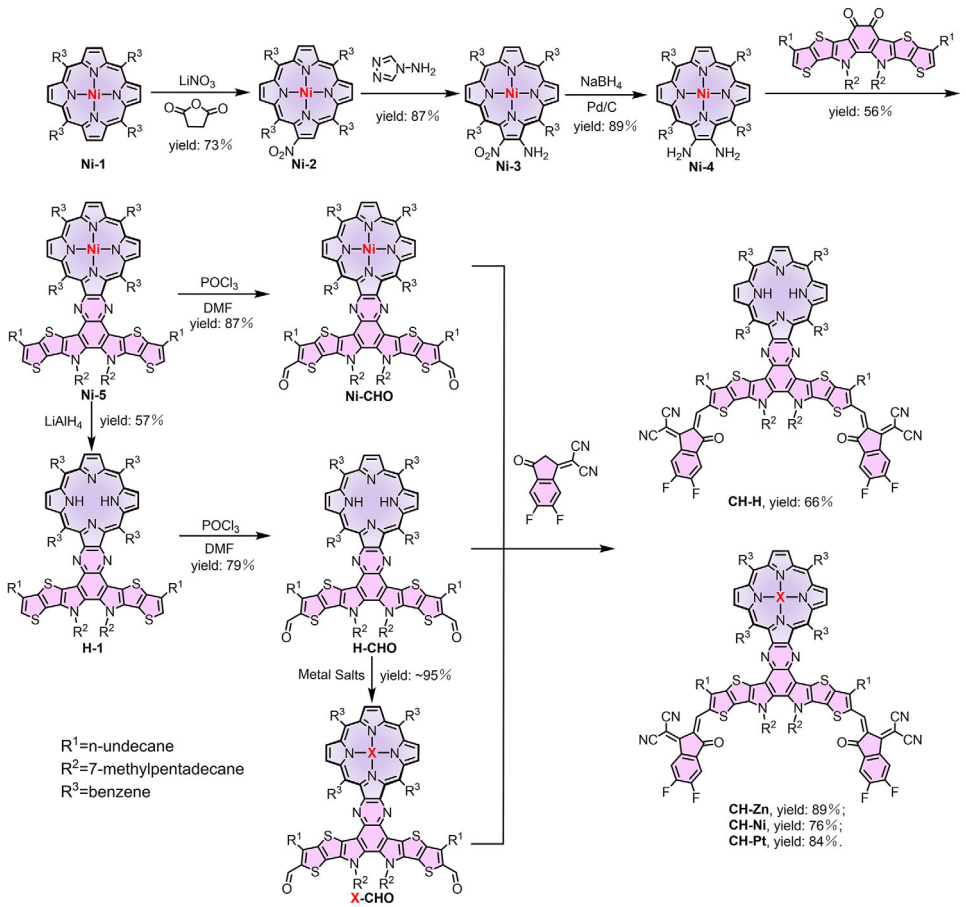

Scheme 1. The synthesized routes to CH—H, CH—Zn, CH—Ni and CH—Pt.

porphyrin bring a large steric hindrance, the porphyrin still greatly participates in molecular packings due to its broad conjugated plane (Figure S13). For example, the E/C packing mode with large intermolecular potentials was observed in both CH—H and CH—Zn (Table S4), contributing a lot for the formation of 3D intermolecular packing network.

The photoluminescence quantum yields (PLQYs, Figures 3a and S15) of CH—H (5.9%) and CH—Pt (3.8%) are markedly larger than that of CH—Zn (0.1%) and CH—Ni (0.2%), which was also evidenced by the decreased densities of steady PLs for CH—Zn and CH—Ni (Figures S16 and S17). The superior luminescent properties of CH—H and CH—Pt are expected to have positive effects on their photovoltaic devices.[45,46] Due to the relatively near HOMO energy levels of SMAs and PM6, the unsatisfied PCEs were achieved by PM6:SMAs-based binary OSCs (Table S5 and Figure S18). By further employing an absorption complementary donor PBDB-T (Figure S19),[47] binary OSCs were fabricated and rendered a PCE of 11.02% for CH—Pt and 10.20% for CH—H, better than that of 7.27% for CH—Ni and 1.89% for CH—Zn (Figure 3b and Table 1). The V_{OC}s of CH—Pt (0.867 V) and CH—H (0.850 V) are larger than that of CH—Ni (0.829 V) and CH—Zn (0.781 V), which benefits from the suppressed non-radiative recombination (Figures S20–S22 and Table S10). More interestingly, the better PCE of 11.56% is further rendered by PM6:PBDB-T:CH—Pt ternary OSCs after introducing PM6 as the third component (Table S16 and Figure S23). Herein, we have demonstrated that the species of metals on SMAs could affect their luminescent properties significantly and provided a valuable exemplification for correlating energy loss of OSCs with luminescent properties of SMAs.[48–50]

The EQEs of CH—Pt and CH—H based OSCs are also much higher than CH—Ni and CH—Zn (Figure 3c), which should be caused by their more efficient exciton dissociation (Figure 3d). This consists with the prolonged exciton lifetimes of CH—Pt and CH—H (Figure 3e), which could facilitate the exciton dissociation even under a smaller energy offset. As regards to the improved FFs of CH—Pt and CH—H based OSCs, the enlarged and more balanced hole/charge mobility should account for that (Figure S24). More excitingly, when further introducing CH—Pt into PM6:BTP-eC9 system as a third component, an excellent PCE of surpassing 20% was achieved (Figures 3f and S25), much better than that using CH—H, CH—Ni, or CH—Zn (also see the EQE plots in Figure S26). The improved nanoscale film morphology of ternary blends should be responsible for this contrasting rise of PCEs (discussed below).

Atomic force microscopy based infrared spectroscopy (AFM-IR) was conducted to unveil the morphology variation with different central metals. All the blends showed the relatively smooth film surface as indicated in Figure S27.

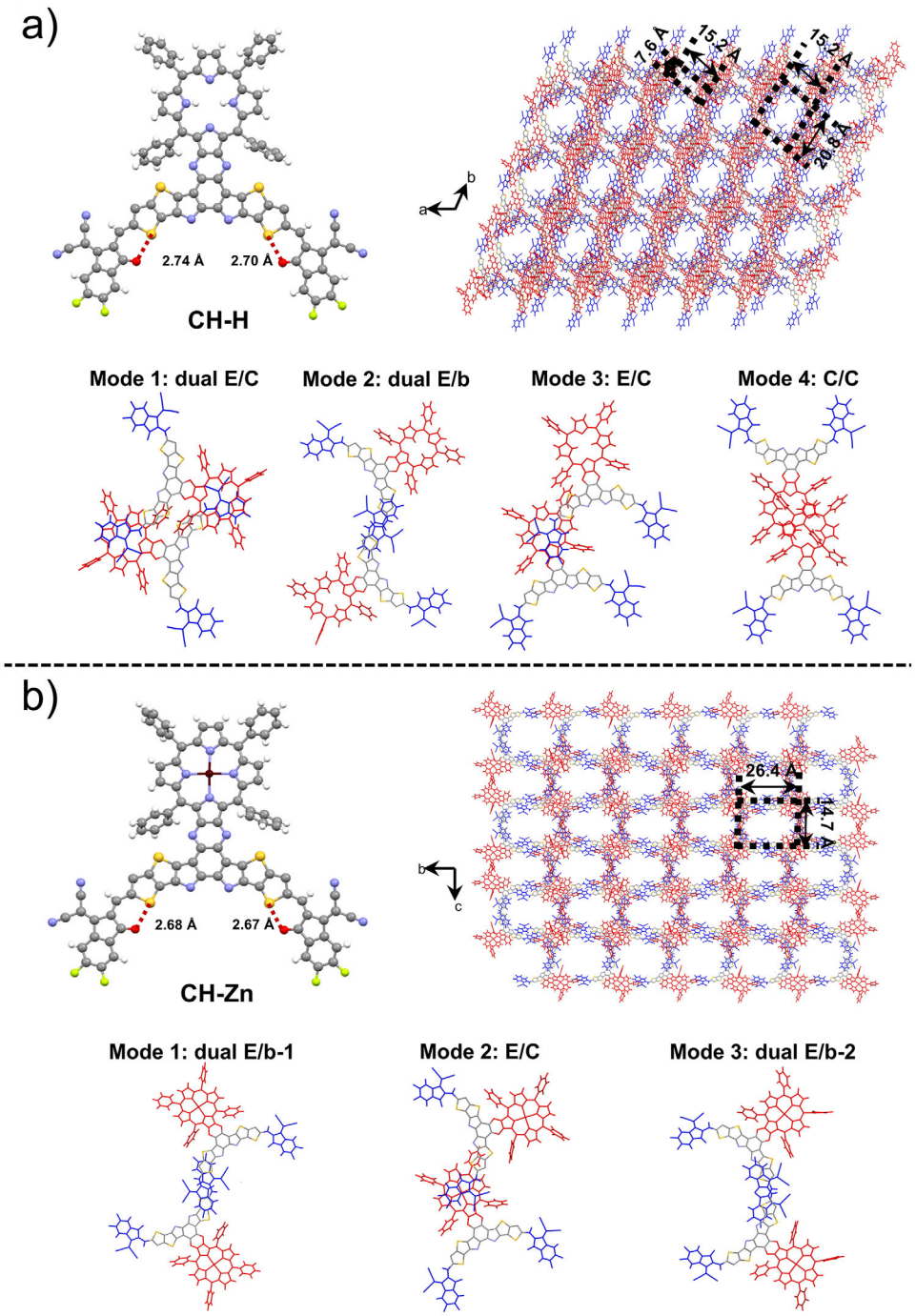

Figure 2. Molecular geometries, molecular packing topological structures and main intermolecular packing modes extracted from single crystals of a) CH—H and b) CH—Zn. Please note that there is a H_2O molecule coordinating with zinc atom as shown in Figure S14, herein we omitted it for a clear presentation.

Moreover, an obvious D/A interpenetrating structures at nanoscale can be observed (Figure 4a), rendering statistical phase separation sizes of 18.1, 23.1, 21.3, and 11.9 nm for CH—H, CH—Zn, CH—Ni, and CH—Pt, respectively (Figures 4b and S28). The more suitable phase separation size of CH—H and CH—Pt are caused by the better miscibility with PBDB-T donor, which could be indicated by the smaller Flory–Huggins interaction parameters (Figure S29 and Table S17). Meanwhile, the more phase interfaces are beneficial for the efficient charge generation (Figure 3d). The 2D grazing incidence wide angle X-ray scattering (GIWAXS) patterns showed the obviously stronger signals around 1.7 $Å^{-1}$ (Figure S30), meanwhile, the slightly enlarged crystal coherence lengths (CCLs, Table S18) for CH—H and CH—Pt blends. This suggests the more ordered molecular packings which help the efficient charge transport in CH—H and CH—Pt

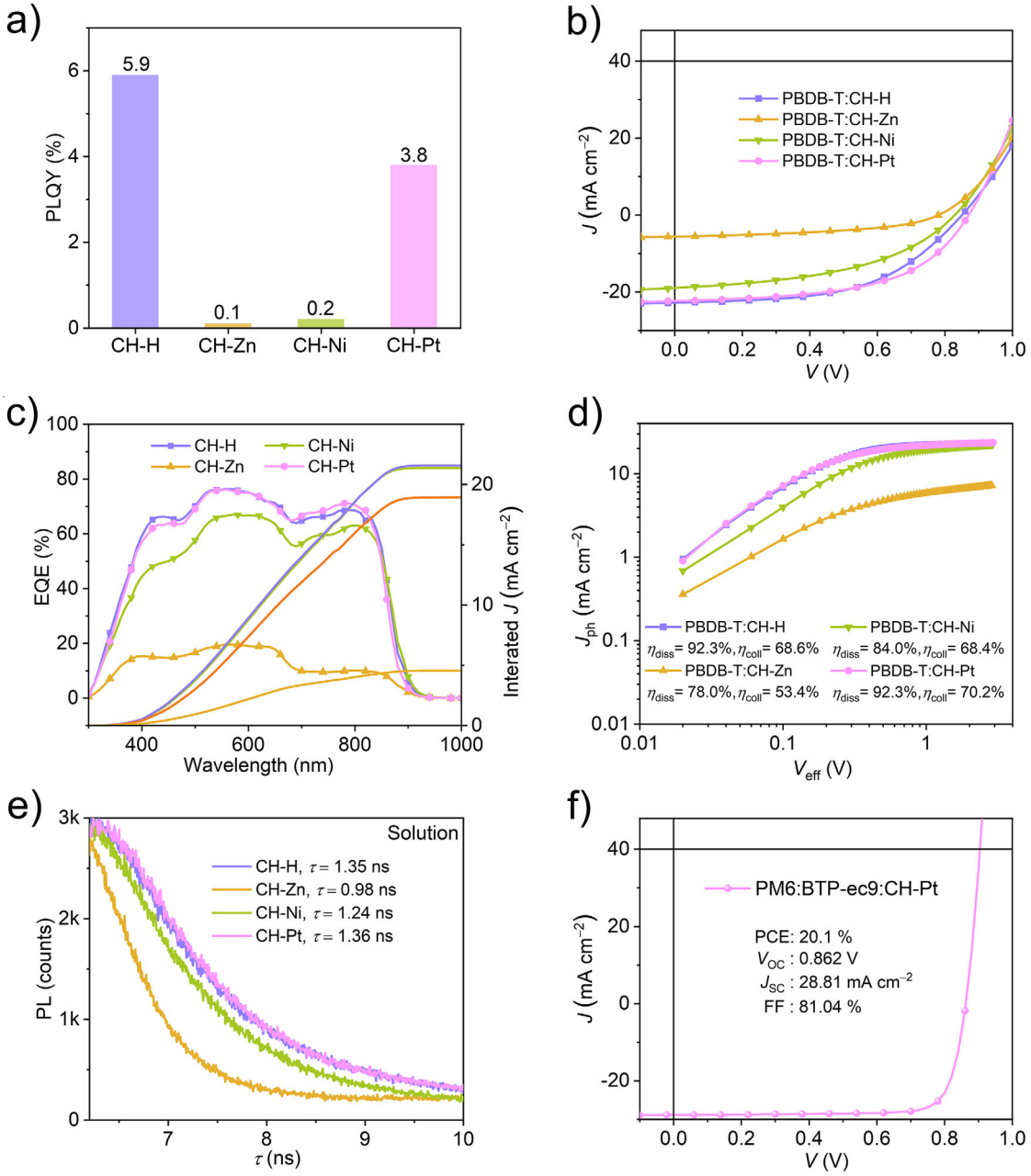

Figure 3. a) Photoluminescence quantum yields (PLQYs) of SMAs films. b) *J–V* curves for PBDT-T:SMAs binary OSCs. (c) EQE plots and integrated J_{SC} curves of binary OSCs. d) J_{ph} versus V_{eff} curves indicating η_{diss} and η_{coll}. e) Time-resolved PL decay traces of SMAs. f) *J–V* curves for PM6:BTP-eC9:CH—Pt ternary OSCs.

blends (Figure S31). When adding CH—Pt into PM6:BTP-eC9 blend, a more obvious D/A interpenetrating fibrillary network can be observed comparing to PM6:BTP-eC9 or PM6:CH—Pt (Figure 4d–f), which should response for the improved PCE of PM6:BTP-eC9:CH—Pt based ternary OSCs.

In conclusion, to explore the prospect of organic metal complexes in photoelectric materials, a rare case of transition metal-containing SMAs is first established by fusing porphyrin core with the widely used S,N-heteroacene of Y-series SMAs. The central metal variation results in the quite different spatial distribution of HOMOs and LUMOs and successfully exerts effects on energy levels, light-harvesting abilities, dipole moments of SMAs. Although the four phenyl groups grafted on porphyrin bring a large steric hindrance, the porphyrin could still participate in the molecular packings greatly and contributes to a desirable 3D intermolecular packing network. More importantly, the Pt-containing SMA of CH—Pt seems to suppress the non-radiative recombination by tuning the luminescent feature of SMAs successfully, providing a valuable exemplification for correlating energy loss of OSCs with luminescent properties of SMAs. Finally, CH—Pt-based ternary organic photovoltaics rendered a first-class PCE surpassing 20%, demonstrating the great prospects of metal complexes in photovoltaic materials.

Table 1: Photovoltaic parameters for OSCs.[a)]

Active Layers	V_{OC} (V)	J_{SC} (mA cm^{-2})	Calc. J_{SC}[b)] (mA cm^{-2})	FF (%)	PCE (%)
PBDB-T: CH—H	0.850 (0.834 ± 0.014)	22.80 (22.53 ± 0.22)	21.86	52.60 (51.21 ± 0.75)	10.20 (9.63 ± 0.27)
PBDB-T: CH—Zn	0.781 (0.772 ± 0.005)	5.34 (5.13 ± 0.10)	4.55	45.31 (46.02 ± 0.97)	1.89 (1.82 ± 0.04)
PBDB-T: CH—Ni	0.829 (0.819 ± 0.006)	18.98 (18.50 ± 0.24)	18.93	46.16 (45.76 ± 0.60)	7.27 (6.92 ± 0.16)
PBDB-T: CH—Pt	0.873 (0.868 ± 0.003)	22.65 (22.03 ± 0.38)	22.14	55.69 (54.84 ± 0.71)	11.02 (10.44 ± 0.23)
PM6:BTP-eC9: CH—H	0.815 (0.804 ± 0.007)	28.27 (27.79 ± 0.26)	27.30	75.93 (74.67 ± 1.08)	17.51 (16.70 ± 0.46)
PM6:BTP-eC9: CH—Zn	0.797 (0.795 ± 0.003)	19.79 (19.05 ± 0.99)	18.87	69.58 (68.12 ± 2.12)	10.97 (10.32 ± 0.66)
PM6:BTP-eC9: CH—Ni	0.818 (0.811 ± 0.004)	27.30 (26.80 ± 0.31)	26.14	70.24 (68.66 ± 1.73)	15.68 (14.92 ± 0.57)
PM6:BTP-eC9: CH—Pt	0.862 (0.861 ± 0.003)	28.81 (28.59 ± 0.17)	27.59	81.04 (80.75 ± 0.33)	20.10 (19.84 ± 0.11)

[a)] The champion and statistical parameters were out/in parentheses, respectively. The statistical ones were derived from 10 devices (Tables S6–S9 and S11–S15). [b)] Current densities afforded by EQE plots.

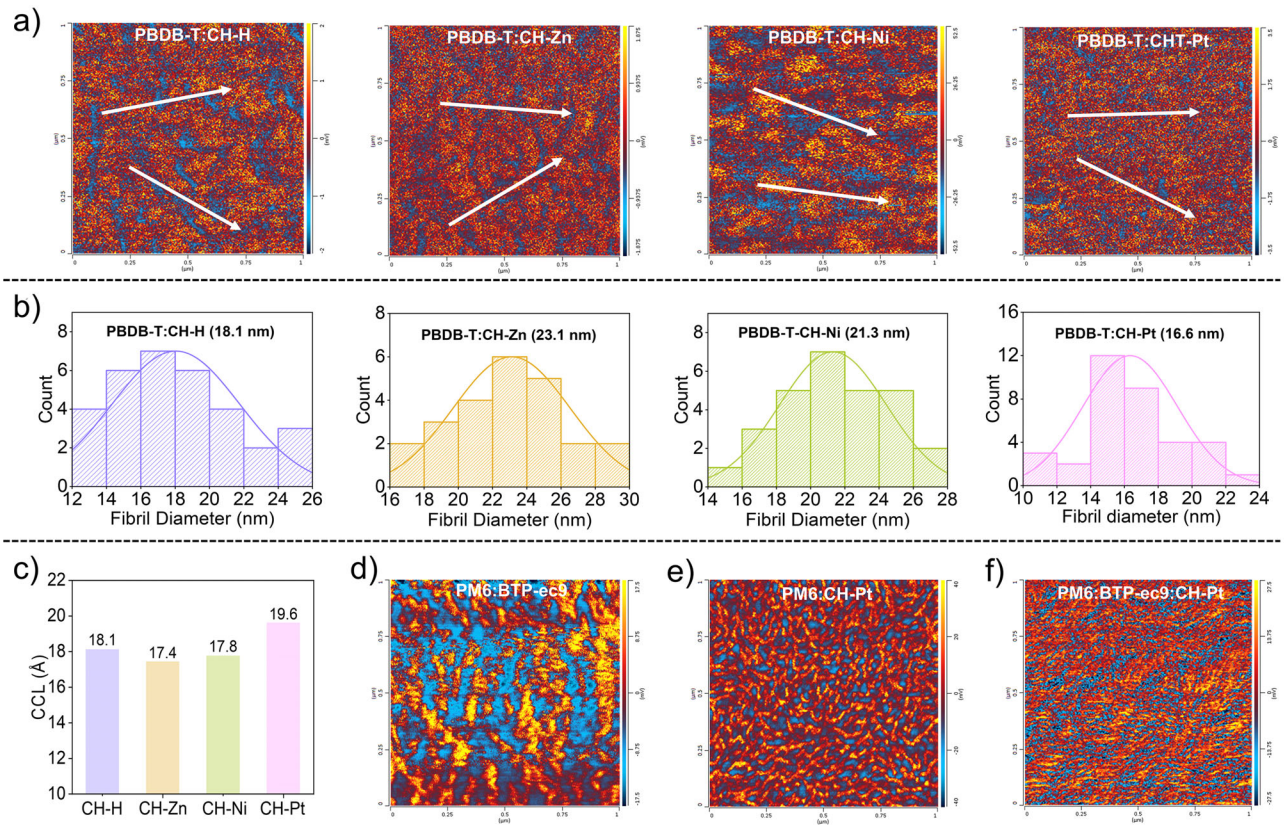

Figure 4. a) AFM-IR images of PBDB-T:SMA blends. The donor and acceptor domains were marked with blue and red colors, respectively. b) Statistical analysis of phase separation sizes in Figure 4a. c) CCLs of D/A blends in out-of-plane direction. d–f) AFM-IR images of PM6:BTP-eC9, PM6:CH—Pt and PM6:BTP-eC9:CH—Pt blends, respectively.

By disclosing the dependency of organic metal complex on intrinsic photovoltaic properties of SMAs, our work also provides a pertinent discussion or guidance to further design of metal-containing SMAs as following: In the current case, the introduction of transition metals into SMAs seems not to inherit the expected features of organic metal complex itself (e.g., the prolonged exciton lifetime, more efficient exciton diffusion, or dissociation, etc.). The primary reason may be that the properties of excited or CT state are still largely determined by the ICT process between

S,N-heteroacene donor and indandione-based electron-deficient terminals, rather than the LMCT of porphyrin-metal rings. This could be clear indicated by the very similar absorption spectrum of CH─H to that of CH─Zn, CH─Pt, etc., especially for their maximum absorption peaks around 768 nm. To fulfill the intrinsic properties of metal complexes in SMAs, the metal complexes should act as the main donor unit on the linear conjugated skeleton rather than the auxiliary central unit. We believe that an easily observable indicator of realizing above goal is quite different absorption spectra from the available acceptors currently. Therefore, although organic metal complexes have great prospects in photovoltaic materials, there is still a long way to go in terms of how to fully demonstrate their unique properties in molecular design.

Supporting Information

Supporting Information is available and contains materials synthesis, device characterization, charge mobility, CV, UV–vis spectra, interface materials (Figure S32), NMR and HR-MS spectra (Figures S33–S52), additional tables, etc.

Acknowledgements

The authors gratefully acknowledge the financial support from Ministry of Science and Technology of the People's Republic of China (National Key R&D Program of China, 2023YFE0210400), National Natural Science Foundation of China (22361132530, 52025033, 52373189, 22479081, 22309090, 22204119, 22474089), Natural Science Foundation of Tianjin (23JCZDJC00140, 23JCZDJC01160) and Haihe Laboratory of Sustainable Chemical Transformations.

Conflict of Interests

The authors declare no conflict of interest.

Data Availability Statement

The data that support the findings of this study are available from the corresponding author upon reasonable request.

Keywords: Electron acceptor · Energy loss · Molecular design · Organic metal complex · Organic photovoltaic

[1] H. Chen, Y. Huang, R. Zhang, H. Mou, J. Ding, J. Zhou, Z. Wang, H. Li, W. Chen, J. Zhu, Q. Cheng, H. Gu, X. Wu, T. Zhang, Y. Wang, H. Zhu, Z. Xie, F. Gao, Y. Li, Y. Li, *Nat. Mater.* **2025**, 1–10.

[2] L. Zhu, M. Zhang, G. Zhou, Z. Wang, W. Zhong, J. Zhuang, Z. Zhou, X. Gao, L. Kan, B. Hao, F. Han, R. Zeng, X. Xue, S. Xu, H. Jing, B. Xiao, H. Zhu, Y. Zhang, F. Liu, *Joule* **2024**, *8*, 3153–3168.

[3] Y. Jiang, S. Sun, R. Xu, F. Liu, X. Miao, G. Ran, K. Liu, Y. Yi, W. Zhang, X. Zhu, *Nat. Energy* **2024**, *9*, 975–986.

[4] S. Guan, Y. Li, C. Xu, N. Yin, C. Xu, C. Wang, M. Wang, Y. Xu, Q. Chen, D. Wang, L. Zuo, H. Chen, *Adv. Mater.* **2024**, *36*, 2400342.

[5] Y. Sun, L. Wang, C. Guo, J. Xiao, C. Liu, C. Chen, W. Xia, Z. Gan, J. Cheng, J. Zhou, Z. Chen, J. Zhou, D. Liu, T. Wang, W. Li, *J. Am. Chem. Soc.* **2024**, *146*, 12011–12019.

[6] Y. Lin, J. Wang, Z.-G. Zhang, H. Bai, Y. Li, D. Zhu, X. Zhan, *Adv. Mater.* **2015**, *27*, 1170–1174.

[7] G. Yu, J. Gao, J. C. Hummelen, F. Wudl, A. J. Heeger, *Science* **1995**, *270*, 1789–1791.

[8] J. Yuan, Y. Zhang, L. Zhou, G. Zhang, H.-L. Yip, T.-K. Lau, X. Lu, C. Zhu, H. Peng, P. A. Johnson, M. Leclerc, Y. Cao, J. Ulanski, Y. Li, Y. Zou, *Joule* **2019**, *3*, 1140–1151.

[9] Y. Li, X. Ru, M. Yang, Y. Zheng, S. Yin, C. Hong, F. Peng, M. Qu, C. Xue, J. Lu, L. Fang, C. Su, D. Chen, J. Xu, C. Yan, Z. Li, X. Xu, Z. Shao, *Nature* **2024**, *626*, 105–110.

[10] S. Li, Y. Jiang, J. Xu, D. Wang, Z. Ding, T. Zhu, B. Chen, Y. Yang, M. Wei, R. Guo, Y. Hou, Y. Chen, C. Sun, K. Wei, S. M. H. Qaid, H. Lu, H. Tan, D. Di, J. Chen, M. Grätzel, E. H. Sargent, M. Yuan, *Nature* **2024**, *635*, 82–88.

[11] Y. Yang, H. Chen, C. Liu, J. Xu, C. Huang, C. D. Malliakas, H. Wan, A. S. R. Bati, Z. Wang, R. P. Reynolds, I. W. Gilley, S. Kitade, T. E. Wiggins, S. Zeiske, S. Suragtkhuu, M. Batmunkh, L. X. Chen, B. Chen, M. G. Kanatzidis, E. H. Sargent, *Science* **2024**, *386*, 898–902.

[12] K. Zhao, Q. Liu, L. Yao, C. Değer, J. Shen, X. Zhang, P. Shi, Y. Tian, Y. Luo, J. Xu, J. Zhou, D. Jin, S. Wang, W. Fan, S. Zhang, S. Chu, X. Wang, L. Tian, R. Liu, L. Zhang, I. Yavuz, H.-f. Wang, D. Yang, R. Wang, J. Xue, *Nature* **2024**, *632*, 301–306.

[13] X. Ru, M. Yang, S. Yin, Y. Wang, C. Hong, F. Peng, Y. Yuan, C. Sun, C. Xue, M. Qu, J. Wang, J. Lu, L. Fang, H. Deng, T. Xie, S. Liu, Z. Li, X. Xu, *Joule* **2024**, *8*, 1092–1104.

[14] Y. Pan, J. Wang, Z. Sun, J. Zhang, Z. Zhou, C. Shi, S. Liu, F. Ren, R. Chen, Y. Cai, H. Sun, B. Liu, Z. Zhang, Z. Zhao, Z. Cai, X. Qin, Z. Zhao, Y. Ji, N. Li, W. Huang, Z. Liu, W. Chen, *Nat. Commun.* **2024**, *15*, 7335.

[15] S. Wu, J. Zhang, Z. Li, D. Liu, M. Qin, S. H. Cheung, X. Lu, D. Lei, S. K. So, Z. Zhu, A. K. Y. Jen, *Joule* **2020**, *4*, 1248–1262.

[16] H. Chen, Y. Zou, H. Liang, T. He, X. Xu, Y. Zhang, Z. Ma, J. Wang, M. Zhang, Q. Li, C. Li, G. Long, X. Wan, Z. Yao, Y. Chen, *Sci. Chi. Chem.* **2022**, *65*, 1362–1373.

[17] A. J. Gillett, A. Privitera, R. Dilmurat, A. Karki, D. Qian, A. Pershin, G. Londi, W. K. Myers, J. Lee, J. Yuan, S.-J. Ko, M. K. Riede, F. Gao, G. C. Bazan, A. Rao, T.-Q. Nguyen, D. Beljonne, R. H. Friend, *Nature* **2021**, *597*, 666–671.

[18] C. Schäfer, R. Ringström, J. Hanrieder, M. Rahm, B. Albinsson, K. Börjesson, *Nat. Commun.* **2024**, *15*, 8705.

[19] D. Qiu, L. Zhang, H. Zhang, A. Tang, J. Zhang, Z. Wei, K. Lu, *J. Mater. Chem. A* **2025**, *13*, 4237–4246.

[20] D. Cai, Y. Ma, K. Xing, J.-Y. Wang, S. Luan, C. Tang, Y. Zhu, S.-C. Chen, Q. Zheng, *Chem* **2024**, *10*, 3131–3147.

[21] H. Rong, P. Ding, S. Qin, Z. Chen, D. Liu, F. Wang, K. Ma, Y. Hu, D. Qian, Z. Ge, *ACS Energy Lett.* **2025**, *10*, 393–402.

[22] H. Fang, Q. Chen, Y. Lin, X. Xu, J. Wang, M. Li, C. Xiao, C. R. McNeill, Z. Tang, Z. Lu, W. Li, *Angew. Chem. Int. Ed.* **2025**, *64*, e202417951.

[23] Y. Lang, H. Lai, Y. Fu, R. Ma, P. W. K. Fong, H. Li, K. Liu, X. Yang, X. Lu, T. Yang, G. Li, F. He, *Adv. Mater.* **2025**, *37*, 2413270.

[24] P. Li, X. Meng, K. Jin, Z. Xu, J. Zhang, L. Zhang, C. Niu, F. Tan, C. Yi, Z. Xiao, Y. Feng, G.-W. Wang, L. Ding, *Carbon Energy* **2023**, *5*, e250.

[25] W. C. H. Choy, W. K. Chan, Y. Yuan, *Adv. Mater.* **2014**, *26*, 5368–5399.

[26] Y.-C. Wei, K.-H. Kuo, Y. Chi, P.-T. Chou, *Acc. Chem. Res.* **2023**, *56*, 689–699.

[27] D. Luo, L. Zhang, J. Zeng, H. Zhang, L. Li, T. Dai, B. Xu, E. Zhou, A. K. K. Kyaw, Y. Chen, W.-Y. Wong, *Adv. Mater.* **2024**, 2410880.
[28] K. Gao, Y. Kan, X. Chen, F. Liu, B. Kan, L. Nian, X. Wan, Y. Chen, X. Peng, T. P. Russell, Y. Cao, A. K. Y. Jen, *Adv. Mater.* **2020**, *32*, 1906129.
[29] J. Yuan, T. Huang, P. Cheng, Y. Zou, H. Zhang, J. L. Yang, S.-Y. Chang, Z. Zhang, W. Huang, R. Wang, D. Meng, F. Gao, Y. Yang, *Nat. Commun.* **2019**, *10*, 570.
[30] Y. Gao, X. Yang, R. Sun, L.-Y. Xu, Z. Chen, M. Zhang, H. Zhu, J. Min, *Joule* **2023**, *7*, 2845–2858.
[31] M. Deng, X. Xu, Y. Duan, W. Qiu, L. Yu, R. Li, Q. Peng, *Adv. Mater.* **2024**, *36*, 2308216.
[32] M. Morisue, M. Nakamura, Y. Miyake, Y. Kashiwagi, S. Watase, T. Hoshino, H. Masunaga, S. Sakurai, S. Sasaki, *Cryst. Growth Des.* **2023**, *23*, 6747–6755.
[33] H. Chen, H. Liang, Z. Guo, Y. Zhu, Z. Zhang, Z. Li, X. Cao, H. Wang, W. Feng, Y. Zou, L. Meng, X. Xu, B. Kan, C. Li, Z. Yao, X. Wan, Z. Ma, Y. Chen, *Angew. Chem. Int. Ed.* **2022**, *61*, e202209580.
[34] T. Hatakeyama, K. Shiren, K. Nakajima, S. Nomura, S. Nakatsuka, K. Kinoshita, J. Ni, Y. Ono, T. Ikuta, *Adv. Mater.* **2016**, *28*, 2777–2781.
[35] X. Li, Y. Wang, G. V. Baryshnikov, I. Sahalianov, H. Ågren, Y. Tanuma, Z. Zhang, C. Qian, M. Cong, T. Yi, H. Wu, *Angew. Chem. Int. Ed.* **2024**, e202422009.
[36] T. Wang, H.-S. Tan, A.-J. Wang, S.-S. Li, J.-J. Feng, *Biosens. Bioelectron.* **2024**, *257*, 116323.
[37] Z. Chen, Y. Xiao, H. Yao, J. Ren, T. Zhang, J. Qiao, S. Zhu, R. Lin, X. Hao, J. Hou, *Adv. Mater.* **2024**, *36*, 2408858.
[38] B. Zou, A. Liang, P. Ding, J. Yao, X. Zeng, H. Li, R. Ma, C. Li, W. Wu, D. Chen, M. Qammar, H. Yu, J. Yi, L. Guo, S. H. Pun, J. E. Halpert, G. Li, Z. Kan, H. Yan, *Angew. Chem. Int. Ed.* **2025**, *64*, e202415332.
[39] E. S. Ryland, M.-F. Lin, M. A. Verkamp, K. Zhang, K. Benke, M. Carlson, J. Vura-Weis, *J. Am. Chem. Soc.* **2018**, *140*, 4691–4696.
[40] G. Ganguly, Z. Havlas, J. Michl, *Inorg. Chem.* **2024**, *63*, 10127–10142.
[41] H. Jiang, P. Hu, J. Ye, R. Ganguly, Y. Li, Y. Long, D. Fichou, W. Hu, C. Kloc, *Angew. Chem. Int. Ed.* **2018**, *57*, 10112–10117.
[42] M. Gervaldo, F. Fungo, E. N. Durantini, J. J. Silber, L. Sereno, L. Otero, *J. Phys. Chem. B* **2005**, *109*, 20953–20962.
[43] C. Li, J. Zhou, J. Song, J. Xu, H. Zhang, X. Zhang, J. Guo, L. Zhu, D. Wei, G. Han, J. Min, Y. Zhang, Z. Xie, Y. Yi, H. Yan, F. Gao, F. Liu, Y. Sun, *Nat. Energy* **2021**, *6*, 605–613.
[44] H. Liang, X. Bi, H. Chen, T. He, Y. Lin, Y. Zhang, K. Ma, W. Feng, Z. Ma, G. Long, C. Li, B. Kan, H. Zhang, O. A. Rakitin, X. Wan, Z. Yao, Y. Chen, *Nat. Commun.* **2023**, *14*, 4707.
[45] H. Lu, D. Li, W. Liu, G. Ran, H. Wu, N. Wei, Z. Tang, Y. Liu, W. Zhang, Z. Bo, *Angew. Chem. Int. Ed.* **2024**, *63*, e202407007.
[46] C. Li, J. Song, H. Lai, H. Zhang, R. Zhou, J. Xu, H. Huang, L. Liu, J. Gao, Y. Li, M. H. Jee, Z. Zheng, S. Liu, J. Yan, X.-K. Chen, Z. Tang, C. Zhang, H. Y. Woo, F. He, F. Gao, H. Yan, Y. Sun, *Nat. Mater.* **2025**, 1–10.
[47] D. Qian, L. Ye, M. Zhang, Y. Liang, L. Li, Y. Huang, X. Guo, S. Zhang, Z. a. Tan, J. Hou, *Macromol.* **2012**, *45*, 9611–9617.
[48] C. e. Zhang, R. Zheng, H. Huang, G. Ran, W. Liu, Q. Chen, B. Wu, H. Wang, Z. Luo, W. Zhang, W. Ma, Z. Bo, C. Yang, *Adv. Energy Mater.* **2024**, *14*, 2303756.
[49] Y. Qiao, X. Liu, Y. Li, X. Guo, C. Li, *J. Mater. Chem. A* **2024**, *12*, 5493–5498.
[50] Y. Jiang, Y. Li, F. Liu, W. Wang, W. Su, W. Liu, S. Liu, W. Zhang, J. Hou, S. Xu, Y. Yi, X. Zhu, *Nat. Commun.* **2023**, *14*, 5079.

Manuscript received: February 25, 2025
Revised manuscript received: March 24, 2025
Accepted manuscript online: March 25, 2025
Version of record online: ■■, ■■

Communication

Photovoltaic Materials

Z. Xu, S. Ding, W. Shi, W. Zhao, X. Cao, Z. Yao*, Y. Guo, G. Long, C. Li, X. Wan, Y. Chen* — **e202504616**

High Performance Electron Acceptors Containing Transition Metals

A novel molecular platform characteristic of multiple transition metals (CH—Zn, CH—Ni, CH—Pt) on conjugated backbones, is first established by fusing porphyrin core with the widely used S,N-heteroacene.